RESEARCH ARTICLE

Ethylenediamine-Controlled Morphological Evolution of Tapered Zn_2GeO_4 Bundles for Light-driven CO_2 Photoreduction

Yiqing Wei[1,*], **Wei Zhao**[2], **Chen Zhuang**[2] **and Yong Zhou**[2,*]

[1] Nanjing University of Industry Technology, Nanjing 210023, China
[2] National Laboratory of Solid-State Microstructures, Collaborative Innovation Center of Advanced Microstructures, School of Physics, Nanjing University, Nanjing 210093, China

Abstract

Morphology engineering stands as a cornerstone strategy to boost the light harvesting and charge transport properties of wide-bandgap oxide photocatalysts. Herein, a Zn_2GeO_4 photocatalyst with a highly symmetric conical bundle architecture is successfully fabricated via modulating the dosage of ethylenediamine (EDA). The introduction of a moderate EDA dosage effectively triggers the anisotropic growth of Zn_2GeO_4, thus constructing a compact and highly ordered conical bundle microstructure (denoted as 4-ZGO). This unique hierarchical morphology not only remarkably shortens the migration pathway of photogenerated charge carriers toward the catalyst surface, but also substantially suppresses bulk-phase charge recombination. Photoelectrochemical characterizations verify that 4-ZGO delivers superior performance in facilitating charge separation and efficient charge migration. As a result, 4-ZGO exhibits exceptional catalytic activity and robust operational stability for photocatalytic CO_2 reduction, affording an impressive 6-hour production yield of 34.97 μmol·g^{-1}.

Keywords: Zn_2GeO_4, ethylenediamine, morphology control, photocatalytic CO_2 reduction.

1 Introduction

The excessive emission of carbon dioxide has driven two intertwined global challenges—accelerating climate change and the depletion of fossil-fuel reserves—spurring extensive research into the catalytic conversion of CO_2 into value-added chemicals as a promising mitigation strategy [1]. Photocatalytic CO_2 conversion using water as the reducing agent has drawn widespread research attention, as this technology realizes the dual value of converting intermittent solar energy into storable chemical energy while synthesizing high-value carbon-based raw materials. However, the inherent chemical inertness of CO_2 molecules, the complex

Submitted: 23 June 2026
Revised: 21 August 2026
Accepted: 29 August 2026
Published: 03 September 2026

Vol. 2, **No.** 3, 2026.
10.62762/JAMR.2026.752860

***Corresponding authors:**
✉ Yiqing Wei
wyq@niit.edu.cn
✉ Yong Zhou
zhouyong1999@nju.edu.cn

Citation
Wei, Y., Zhao, W., Zhuang, C., & Zhou, Y. (2026). Ethylenediamine-Controlled Morphological Evolution of Tapered Zn_2GeO_4 Bundles for Light-driven CO_2 Photoreduction. *Journal of Advanced Materials Research*, 2(3), 251–261.

multi-electron transfer processes, and the competitive reactions all impose extremely high requirements on the catalysts [2, 3]. In particular, efficient carrier utilization and precise active-site engineering are recognized as decisive factors governing catalytic selectivity and conversion efficiency [4, 5]. Wide bandgap semiconductors possess a strong redox potential, have sufficient thermodynamic driving force to achieve deep catalytic reactions, and usually have excellent chemical stability and resistance to light corrosion. As a typical wide bandgap semiconductor, Zn_2GeO_4 possesses an energy band structure suitable for CO_2 reduction, and it has excellent resistance to light corrosion. It is an ideal material for photocatalytic CO_2 reduction, and its surface has demonstrated strong CO_2 adsorption and activation capabilities [6–9]. Although its conduction band potential is sufficiently negative, providing a strong thermodynamic driving force for reduction catalytic reactions, the overall photocatalytic efficiency is severely limited by the short carrier diffusion length [10–12]. To overcome these limitations, multiple strategies have been pursued: elemental substitution and solid-solution engineering have been explored to modulate the band structure and improve charge utilization in germanate-based oxide photocatalysts [13], while considerable efforts have also been devoted to constructing the morphology of Zn_2GeO_4 and effectively reducing the distance over which photogenerated carriers migrate from the generation site to the surface reaction site, thereby enhancing the charge separation efficiency [14–17]. Heterojunction construction with complementary semiconductors represents another effective strategy to further boost the photocatalytic activity of Zn_2GeO_4 [18].

In achieving precise control over crystal growth, the solvothermal method has become a mainstream strategy for constructing semiconductors with specific morphologies due to its controllable reaction environment and ability to readily induce preferential growth on certain crystal facets [19]. Beyond Zn_2GeO_4, morphology engineering of other oxide semiconductors such as ZnO has also been demonstrated to substantially enhance photocatalytic CO_2 reduction performance [20, 21], further underscoring the universality of morphology control as a performance-boosting strategy. Among the available synthetic handles, the nature and concentration of structure-directing agents play a pivotal role. Clarifying the multiple regulatory effects of EDA on crystallization is therefore helpful in elucidating the mechanism of morphology regulation. EDA can act as a bidentate ligand and coordinate with Zn^{2+} ions, regulating the release rate of free zinc ions. It is speculated that EDA may modify the surface energy of certain crystal planes to trigger anisotropic crystal growth, which is commonly ascribed to facet-preferential adsorption in related literature [22–24]. Moreover, EDA can regulate the polarity and viscosity of the solvent, affecting the diffusion of precursors and the assembly of crystal nuclei. Collectively, EDA may exert synergistic modulation effects on multiple stages including nucleation, crystal growth, and nucleus assembly.

In this work, a solvothermal method was employed to systematically investigate the regulatory effects of solvent composition on the crystal growth habits, micro-morphology, and photoresponse characteristics of Zn_2GeO_4 by precisely adjusting the volume ratio of water to EDA in the precursor solution. The experiment shows that an appropriate dose of EDA can effectively promote the anisotropic growth of Zn_2GeO_4, and a compact and highly ordered cone-bundle microstructure has been prepared. Photocatalytic CO_2 reduction experiments demonstrate that the well-defined cone-bundle Zn_2GeO_4 exhibits superior catalytic activity: within a 6-hour reaction period, the cumulative yield of the primary product CO reached 34.97 $\mu mol \cdot g^{-1}$, with an average generation rate of approximately 5.83 $\mu mol \cdot g^{-1} \cdot h^{-1}$, and the catalytic activity continuously increased over time; meanwhile, the secondary product CH_4 steadily accumulated to 5.64 $\mu mol \cdot g^{-1}$. This work provides a theoretical foundation and experimental support for systematically exploring the mechanism of ligand-assisted crystal growth and the rational design of efficient Zn_2GeO_4 photocatalysts.

2 Experimental Section

2.1 Synthesis of Zn_2GeO_4

Zn_2GeO_4 powders were synthesized by a solvothermal method. GeO_2 (0.18 g, 2.5 mmol) and zinc acetate dihydrate ($Zn(CH_3COO)_2 \cdot 2H_2O$, 1.10 g, 5.0 mmol) were added to a mixed water/EDA solvent. The deionized-water volume was fixed at 10 mL, whereas the EDA volume was 3, 4, 5, or 6 mL. Each mixture was magnetically stirred at room temperature for 40 min and transferred into a 25 mL Teflon-lined stainless-steel autoclave. The sealed autoclave was heated at 180 °C for 12 h and then allowed to cool naturally

to room temperature. The products were collected by centrifugation at 8000 rpm for 3 min, washed alternately by ultrasonication and centrifugation, three times with absolute ethanol and twice with deionized water, and vacuum-dried at 60 °C for 12 h. The powders prepared with 3, 4, 5, and 6 mL EDA are denoted as 3-ZGO, 4-ZGO, 5-ZGO, and 6-ZGO, respectively. The detailed solvent compositions and EDA/H_2O volume ratios used for the synthesis of the four Zn_2GeO_4 samples are summarized in Table 1. Commercial Zn_2GeO_4 (Yanyibao, purity ≥99%) was used without further purification. The as-received commercial sample consists of irregular bulk particles without well-defined morphological features.

Table 1. Synthesis parameters for different Zn_2GeO_4 samples.

Sample	H_2O (mL)	EDA (mL)	EDA/H_2O ratio
3-ZGO	10	3	0.3
4-ZGO	10	4	0.4
5-ZGO	10	5	0.5
6-ZGO	10	6	0.6

2.2 Structural, Morphological, and Optical Characterization

The morphology of the as-prepared samples was characterized using field emission scanning electron microscopy (FESEM, FEI NOVA NanoSEM 230). The crystal structure was analyzed by X-ray diffraction (XRD, Ultima III, Rigaku) with Cu Kα radiation ($\lambda = 0.15406$ nm). UV-visible diffuse reflectance spectra (UV-vis DRS) were collected on a Shimadzu UV-2550 spectrophotometer.

2.3 Photoelectrochemical Measurements

Photoelectrochemical performances of all samples were measured on a combined system consisting of a 300 W Xe arc lamp (100 mW cm^{-2}, FX 300, Beijing PerfectLight) as the simulated solar light source and an electrochemical workstation (CHI-660E, Shanghai Chenhua). A standard three-electrode configuration was adopted for all tests, with the as-fabricated sample as the working electrode, a Pt plate as the counter electrode, and Ag/AgCl (saturated KCl) as the reference electrode. A 0.5 M Na_2SO_4 aqueous solution (pH = 8.6) was used as the electrolyte.

2.4 Photocatalytic CO_2 Reduction

Photocatalytic CO_2 reduction experiments were carried out at ambient temperature in a gas-tight closed reaction system. In a typical run, 100 mg of the as-prepared powder sample was uniformly dispersed at the bottom of the reactor (irradiation area ~4.91 cm^2). The whole system was evacuated repeatedly to completely eliminate residual air. Subsequently, high-purity CO_2 (99.999%) was introduced into the reactor until atmospheric pressure was reached, followed by injection of 0.4 mL deionized water as the proton source. A 300 W Xe lamp was used as the simulated solar light source, and the reaction temperature was kept constant throughout the test via a circulating water cooling jacket. During the 6-hour continuous irradiation, 1 mL of gas was extracted from the headspace of the reactor every hour, and the gaseous product composition was analyzed by gas chromatography (GC 8890, Agilent Technologies, USA) equipped with a flame ionization detector (FID) and a thermal conductivity detector (TCD). Furthermore, multiple blank control experiments were carried out to exclude carbon contamination derived from EDA decomposition. No CO or CH_4 was detected in the dark reaction without light irradiation. Negligible CO and CH_4 were observed for a pure EDA solution under identical illumination in the photolysis blank test, and no CO production occurred when CO_2 was substituted by high-purity N_2 in the N_2-atmosphere blank experiment.

3 Results and Discussion

The XRD patterns of the four sample groups are presented in Figure 1, with highly consistent overall profiles and characteristic peaks. All distinguishable diffraction peaks can be indexed to the triclinic willemite-type Zn_2GeO_4 structure (PDF#11-0687) by reference to previously reported XRD patterns for this phase [25], and no extra diffraction signals assigned to GeO_2, ZnO, or other possible by-products are detected in the patterns. This result indicates that within the studied EDA dosage range, precursors can be fully converted under solvothermal conditions, and no impurity phases are formed regardless of the solvent composition. It is thus confirmed that high-purity Zn_2GeO_4 crystals are successfully synthesized in all four groups of experiments. Among all the diffraction peaks, only the intensity of the (220) crystal plane peak first increases and then decreases as the EDA content increases. The change in the intensity of this (220) diffraction peak is likely related to the change in crystal growth orientation or assembly mode caused by the variation in EDA content. This change merely reflects the relative adjustment in the development degree of different crystal planes and does not affect the phase purity of the product.

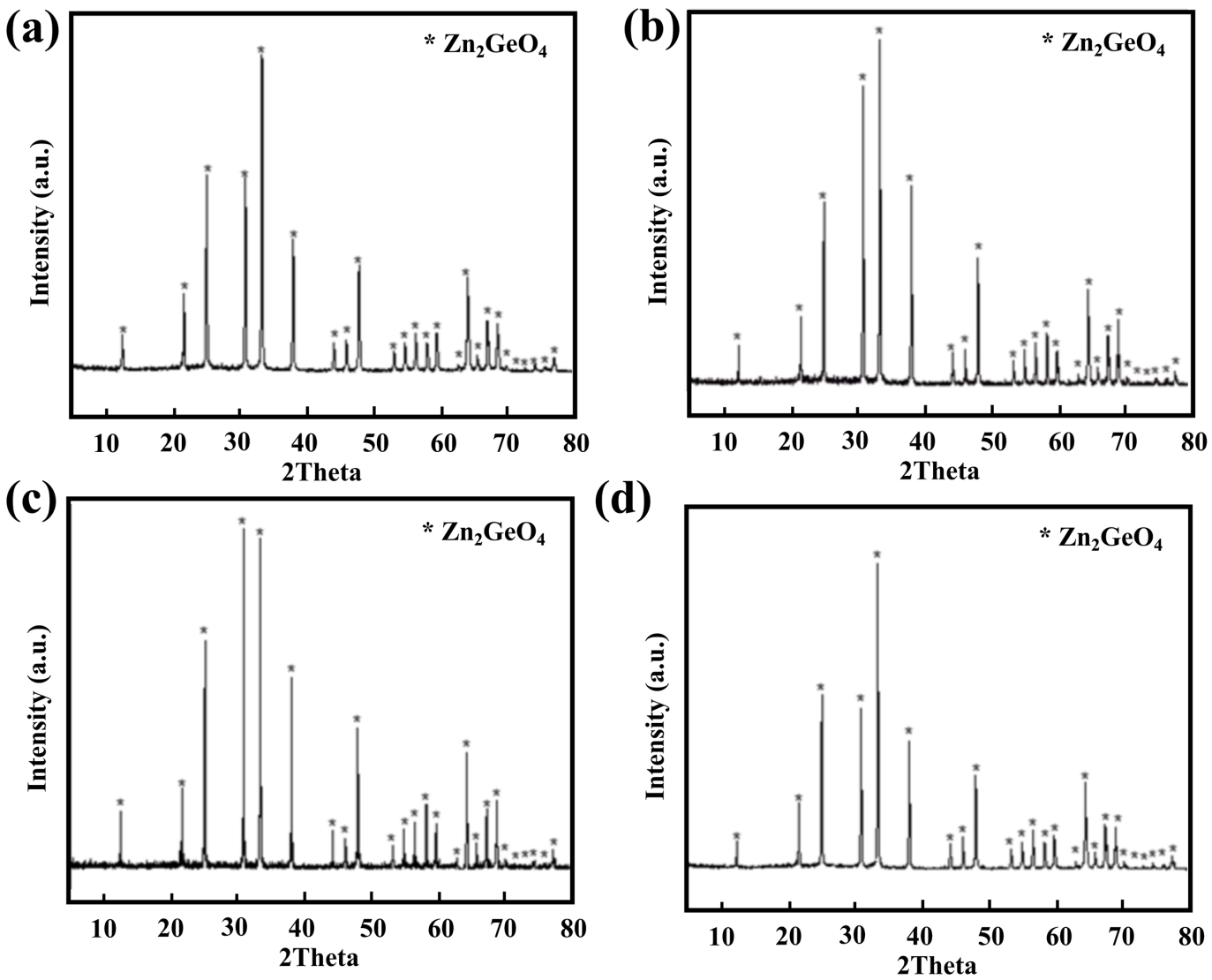

Figure 1. XRD patterns of (a) 3-ZGO, (b) 4-ZGO, (c) 5-ZGO, and (d) 6-ZGO.

To elucidate the morphology-directing role of EDA in the growth of Zn_2GeO_4 crystals, SEM was employed to characterize the microstructures of samples synthesized with different EDA dosages. As presented in Figure 2, all four groups of samples (3-ZGO, 4-ZGO, 5-ZGO and 6-ZGO) exhibit uniform layer-stacked rod-like architectures: nanorods grow directionally along the one-dimensional axial direction and closely stack to form micron-sized rod bundles, verifying that pure-phase layered Zn_2GeO_4 crystals can be obtained under all the investigated experimental conditions. 3-ZGO synthesized at a low EDA dosage (Figures 2(a) and 2(b)) presents a bundle-like conical architecture, which is assembled by relatively thick one-dimensional nanorods with oriented alignment along the axial direction. As the EDA dosage increases (4-ZGO, Figures 2(c) and 2(d)), the crystal growth becomes more uniform. The resulting structure consists of ultrafine one-dimensional nanorods stacked in a parallel fashion, with a significantly narrower particle size distribution. There are obvious voids between the nanorods, forming continuous pore channels, which have a larger specific surface area and a smooth material transfer path. The fine nanoscale building units shorten the migration distance of the light-excited carriers, while the ordered one-dimensional array provides a continuous charge transmission channel. These structural advantages can significantly enhance the separation effect of photogenerated carriers, expose sufficient accessible active sites, and thus render this structure superior in the photocatalytic CO_2 reduction reaction. When the EDA dosage is further increased (5-ZGO, Figure 2(e)), excessive ligands may lead to excessively high solution viscosity and a significant shift in the coordination equilibrium, which hinders the diffusion and transport

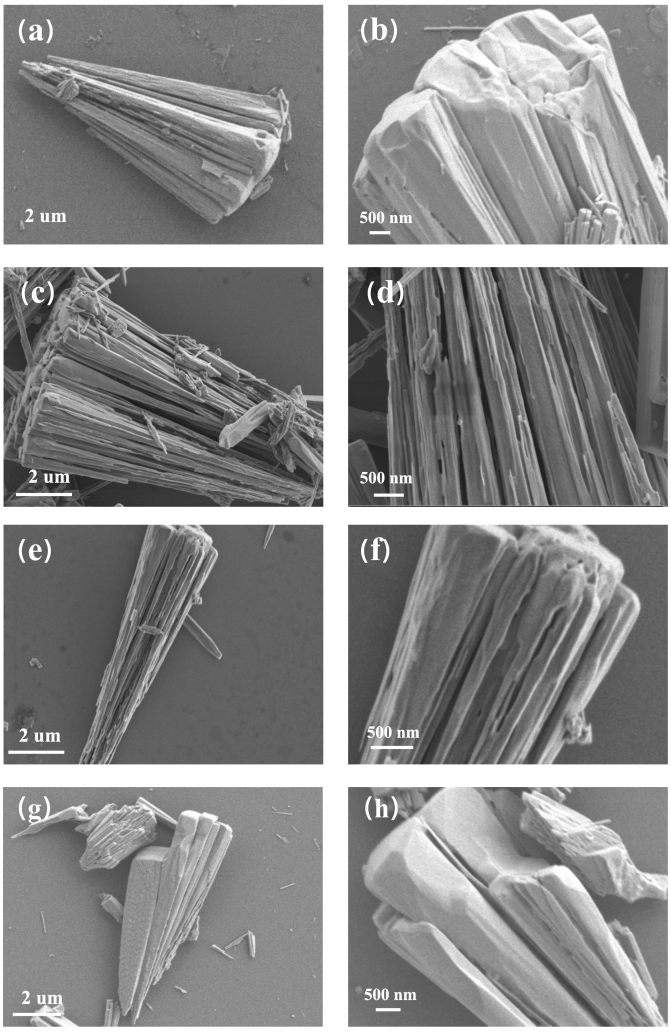

Figure 2. SEM images of (a, b) 3-ZGO, (c, d) 4-ZGO, (e, f) 5-ZGO, and (g, h) 6-ZGO.

of reaction precursors and suppresses crystal growth kinetics. This is manifested as fracture and peeling at the edges of the microbundles (Figure 2(f)) and a decrease in size uniformity, indicating that an excessively high EDA concentration will destroy the ideal growth environment for crystals. When the EDA addition is further raised to an excessive level (6-ZGO, Figures 2(g) and 2(h)), the morphological integrity of the product is impaired: although the basic bundle-like contour is retained, the edge fragmentation and peeling of the microbundles are more prominent, and the size uniformity further decreases. This phenomenon can also be attributed to the increase in solution viscosity and the shift of coordination equilibrium caused by excessive EDA, which interferes with the normal growth process of crystals. EDA plays a dual regulatory role during the growth process of the Zn_2GeO_4 crystal. On one hand, it acts as a chelating agent to control the release rate of Zn^{2+}. On the other hand, based on the morphological evolution and the descriptions in previous literature, EDA can regulate the self-assembly and anisotropic crystal growth process via its coordination template effect [22–24, 26].

Figure 3(a) displays the UV-vis diffuse reflectance absorption spectra of Zn_2GeO_4 samples synthesized at different EDA concentrations. All samples exhibit strong light absorption characteristics in the ultraviolet region, with two distinct absorption peaks clearly observed in the spectra (located at approximately 210 nm and 255 nm, respectively) [11, 27]. This is typically attributed to complex electronic transition processes within the material, specifically the charge transfer transitions from O 2p to Zn 4s/Ge 4s orbitals. Notably, the light absorption behavior of the samples varies significantly with the EDA concentration. The 4-ZGO sample shows the highest absorbance intensity at these two characteristic peaks. This enhanced light-harvesting capability is closely related to its microscopic morphology. As revealed by the SEM results, 4-ZGO possesses a highly ordered and dense layered assembly structure. This unique structure not only helps minimize light scattering losses but may also extend the optical path length through multiple reflection effects, thereby improving photon utilization efficiency. In contrast, the light absorption capabilities of 3-ZGO (due to its relatively loose structure) and 6-ZGO (due to structural damage) are both weakened to a certain extent, accompanied by a relative blue-shift in their absorption edges, reverting to a wider intrinsic band gap state. To quantitatively evaluate the impact of EDA dosage on the electronic structure, Tauc plots are constructed. The results reveal that the EDA concentration significantly modulates the optical band gap. As shown in Figure 3(b), the absorption edge of the 4-ZGO sample shows the most significant red shift, and the calculated band gap is the smallest, approximately 4.63 eV; the absorption edges of the 5-ZGO and 6-ZGO samples exhibit a progressive blue-shift, and the band gaps increase to approximately 4.67 eV and 4.68 eV, respectively. Thus, it can be concluded that the optimized energy band structure and superior light capture ability of the 4-ZGO sample lay a solid foundation for its excellent photocatalytic CO_2 reduction activity. To probe the transport of photogenerated carriers, transient photocurrent responses were recorded under chopped illumination. As shown in Figure 3(c), both 3-ZGO and 6-ZGO exhibit low photocurrent densities, pointing to rapid electron–hole recombination, most likely caused by poor crystallinity or structural defects.

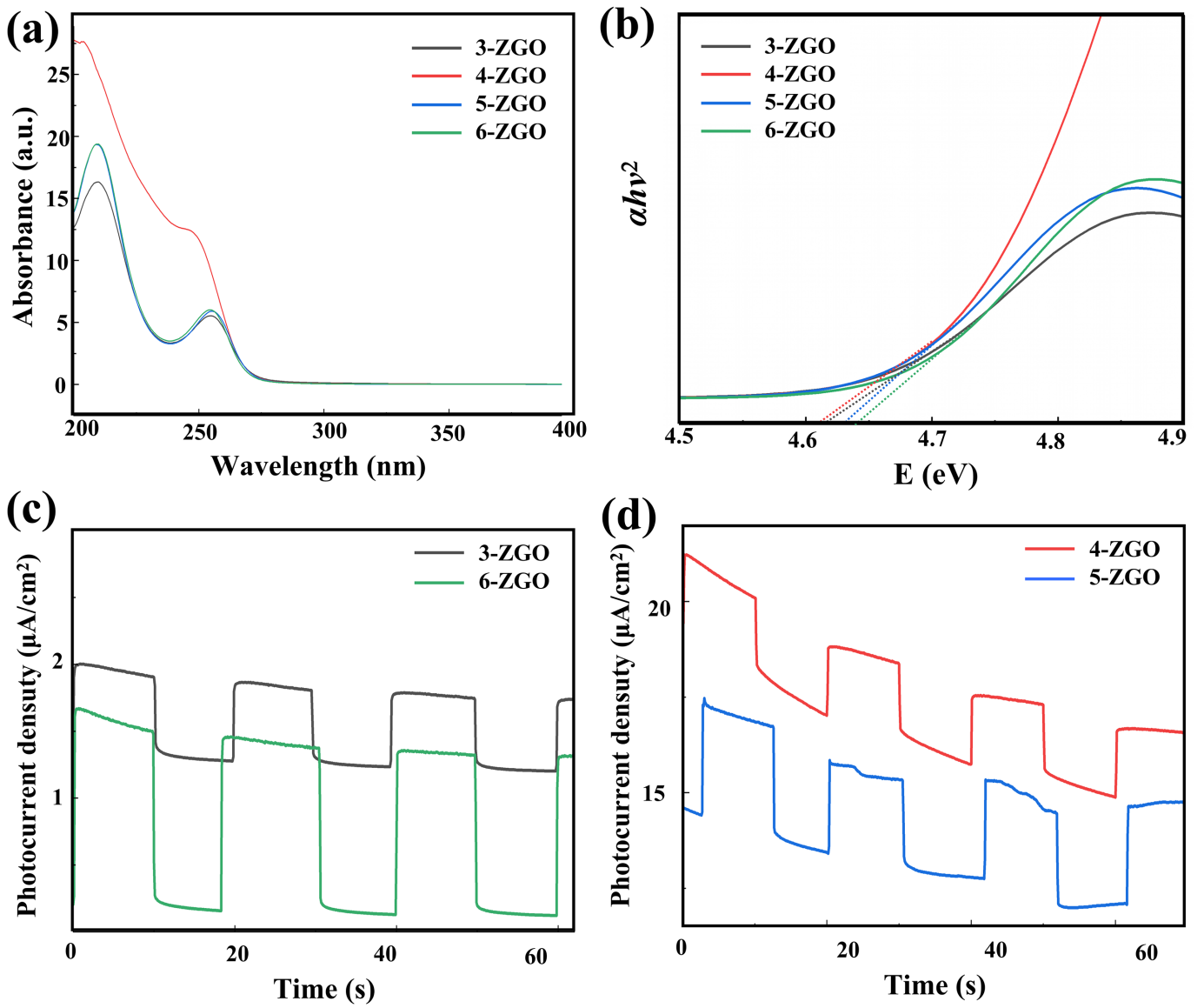

Figure 3. (a) UV-vis absorption spectra and (b) Tauc plots; photocurrent density-time curves of (c) 3-ZGO and 6-ZGO, and (d) 4-ZGO and 5-ZGO.

Conversely, Figure 3(d) shows a marked increase in photocurrent density for 4-ZGO and 5-ZGO. Notably, 4-ZGO gives the highest photocurrent density, roughly one order of magnitude larger than those of 3-ZGO and 6-ZGO. This robust, reproducible photoresponse indicates that the optimized morphology of 4-ZGO promotes efficient carrier separation and transport to surface active sites, a conclusion that is consistent with the enhanced light harvesting and that underpins its superior photocatalytic performance.

The BET specific surface areas and N_2 adsorption-desorption isotherms of EDA-tuned Zn_2GeO_4 samples are shown in Figure 4(a). All samples exhibit Type-IV adsorption isotherms with a distinct rise in adsorbed volume at high relative pressure, indicating the presence of interparticle pore structures in the samples. The BET specific surface areas of the samples are 1.0325 m^2/g for 3-ZGO, 2.6468 m^2/g for 4-ZGO, 0.2335 m^2/g for 5-ZGO, and 1.3992 m^2/g for 6-ZGO. Among them, 4-ZGO possesses the largest specific surface area, which can provide more reactive active sites. Meanwhile, its higher total pore volume facilitates the transport of CO_2 reactants. Therefore, varying EDA content can modulate the microstructure of the material, and further alter the specific surface area and pore characteristics of the samples.

Figure 4(b) presents the product yields and their time-dependent evolution during photocatalytic CO_2 reduction over various catalysts. CO and CH_4 are the major products for 4-ZGO, whereas CO serves as the dominant product for 3-ZGO, 5-ZGO

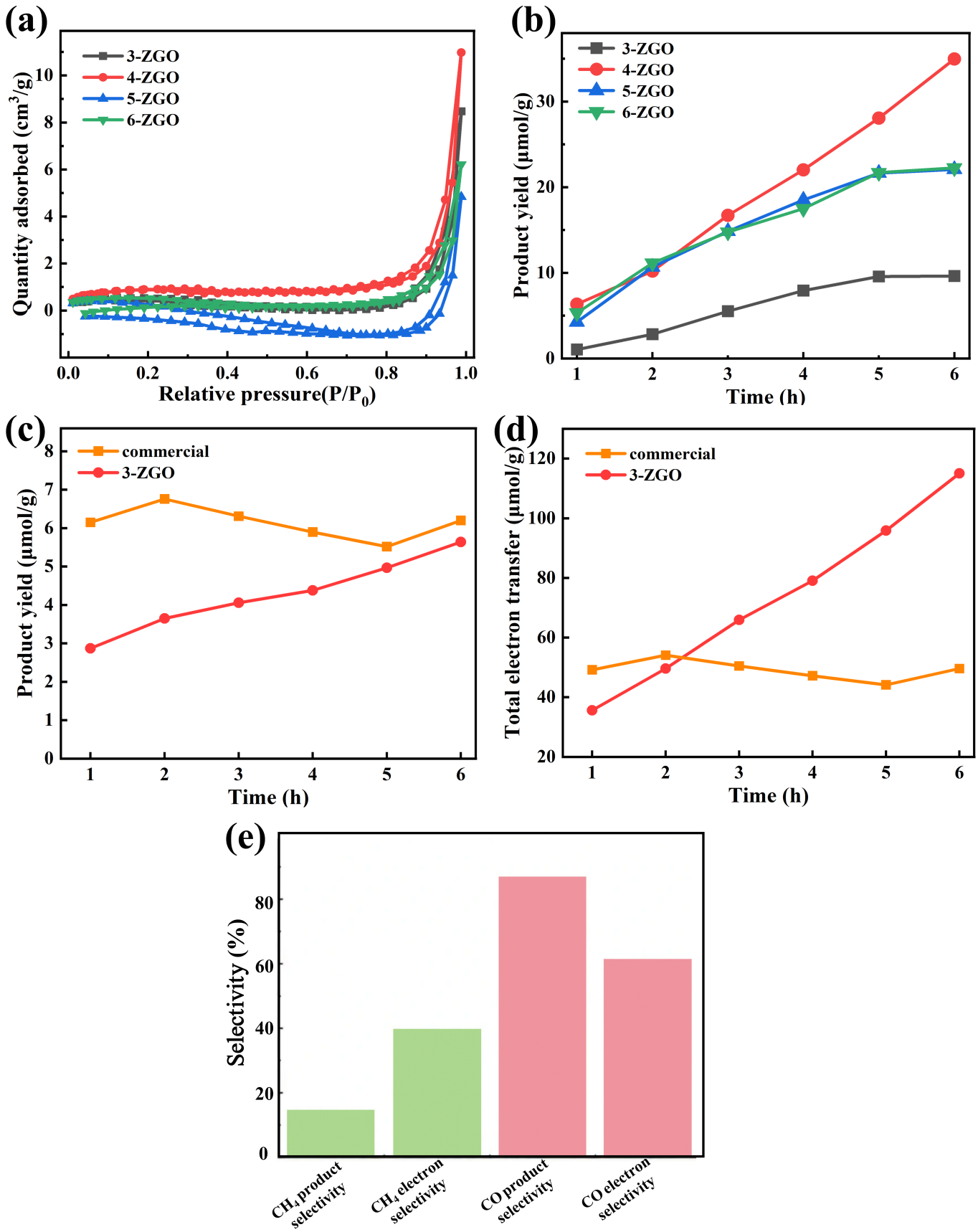

Figure 4. (a) N_2 adsorption-desorption isotherms; (b) time-dependent cumulative CO yield during photocatalytic CO_2 reduction; (c) time-dependent cumulative CH_4 yield of photocatalytic CO_2 reduction over 4-ZGO and the commercial sample under irradiation; (d) total electron transfer of 4-ZGO and the commercial sample; (e) product selectivity and electron selectivity of 4-ZGO.

Table 2. Comparison of CO_2 photoreduction performance of various Zn_2GeO_4-based photocatalysts.

Photocatalyst	Synthetic method	Incident source	Activity (μmol·g^{-1}·h^{-1})	Reference
Zn_2GeO_4	**Solvothermal method**	**Xe lamp (300 W)**	**CO: 5.83; CH_4: 0.94**	**This work**
Zn_2GeO_4	Solvothermal method	Simulated sunlight	CO: 5.3	[19]
20% Zn_2GeO_4/ZIF-67	Solvothermal method	Xe lamp (300 W)	CO: 4.08	[28]
Zn_2GeO_4/MgMOF74	Solvothermal method	Xe lamp (300 W)	CO: 1.44	[29]
Zn_2GeO_4:Er^{3+}/g-C_3N_4	Hydrothermal method	Xe lamp (300 W)	CO: 6.8; CH_4: 10.4	[30]
Zn_2GeO_4	Solvothermal method	Xe lamp (300 W)	CO: 20.81	[31]

and 6-ZGO. For 4-ZGO, both CO and CH_4 yields increase approximately linearly with irradiation time, reaching 34.97 μmol·g^{-1} and 5.64 μmol·g^{-1} after 6 h reaction, which demonstrates its excellent photocatalytic stability under long-term operation. 5-ZGO and 6-ZGO exhibit moderate catalytic activity with cumulative CO yields of 22.08 μmol·g^{-1} and 22.25 μmol·g^{-1} at 6 h, while the product-formation rates of both samples decay at later reaction stages. 3-ZGO shows the poorest CO-producing capability, delivering only 9.62 μmol·g^{-1} of CO after 6 h, and the CO yield accumulation almost stagnates after 5 h. These results reveal that 4-ZGO possesses superior CO_2-reduction catalytic performance. Hydrogen evolution is a major competing side-reaction in aqueous-phase CO_2 photoreduction. In this work, continuous CO_2 purging was performed over the entire photocatalytic reaction to increase the CO_2 concentration at the solid-liquid interface of the catalyst. This strengthens the competition between CO_2 and protons for photogenerated electrons and thus suppresses hydrogen evolution. Meanwhile, the morphology of Zn_2GeO_4 can be modulated by optimizing synthetic conditions, and the obtained Zn_2GeO_4 kinetically favors CO_2 photoreduction. Consequently, no H_2 product was detected in our experiments.

To further evaluate its catalytic merit, 4-ZGO was compared with commercial Zn_2GeO_4. The commercial sample yields CH_4 of approximately 6.2 μmol·g^{-1} after 6 h, which is close to that of 4-ZGO (5.64 μmol·g^{-1}), while its CO yield remains negligible under the same conditions. More importantly, benefiting from its considerable CO production, 4-ZGO achieves a much higher total yield of reduction products. It further confirms that 4-ZGO not only enables efficient photogenerated-charge separation (consistent with transient photocurrent results), but also possesses favorable surface features for multi-path CO_2 reduction, realizing highly selective conversion toward CO. To quantitatively assess the charge utilization efficiency of catalysts during the photocatalytic CO_2 reduction reaction, total electron transfer amounts at different time intervals were calculated based on product yields, with results summarized in Figure 4(d). The 4-ZGO sample exhibits a prominent and continuously increasing electron transfer capacity. As the reaction proceeds, its total transferred electron amount rises steadily from 35.64 μmol·g^{-1} at the 1-hour mark to 115.06 μmol·g^{-1} at 6 hours, which is much higher than that of the commercial Zn_2GeO_4. This result demonstrates that the as-developed catalyst can effectively boost the separation and migration of photoexcited charge carriers, and sustainably drive the multi-electron reduction reactions. This significant difference confirms that 4-ZGO outperforms the commercial counterpart in terms of exposed photocatalytic active sites and charge transfer kinetics, thus enabling higher product selectivity and conversion efficiency. Figure 4(e) compares the products and electron selectivity of the 4-ZGO samples during the photocatalytic CO_2 reduction process. The 4-ZGO samples exhibit a high CO product selectivity (86.1%), while the CH_4 selectivity is only 13.9%. In terms of electron selectivity, CO accounts for 60.8%, which is much higher than the 39.2% of CH_4. This selectivity change indicates that the morphology optimization not only exposes more active crystal faces conducive to the two-electron CO pathway, but also enhances the material's selectivity for CO. To assess the CO_2

photoreduction performance of our as-prepared Zn_2GeO_4, representative reported Zn_2GeO_4-based photocatalysts are summarized in Table 2. Given the variations in synthetic methods, incident sources and activity across different investigations, the catalytic activity achieved in this work is reasonable and comparable for Zn_2GeO_4-based photocatalytic CO_2 reduction.

4 Conclusion

This work successfully fabricated cone-bundle-shaped Zn_2GeO_4 photocatalysts with tunable morphology via modulating EDA dosage during the solvothermal synthesis. EDA dosage is identified as a dominant factor governing crystal morphology: a moderate EDA content induces the formation of dense, highly ordered cone-bundle architectures, while insufficient or excessive EDA gives rise to loose or structurally defective products. This optimized microstructure endows the 4-ZGO sample with exceptional optoelectronic properties: it not only features a narrower band gap and enhanced light-harvesting capability, but also delivers a transient photocurrent density far exceeding those of other control samples, verifying its highly efficient charge carrier migration. In the photocatalytic CO_2 reduction reaction, 4-ZGO exhibits remarkable catalytic activity and long-term cycling stability. Collectively, the dense layered structure constructed via EDA-mediated regulation accounts for the substantially improved photocatalytic performance of Zn_2GeO_4, as this structure optimizes the electronic structure of the material and facilitates efficient charge utilization.

Data Availability Statement

Data will be made available on request.

Funding

This work was supported by the Start-up Fund for New Talented Researchers of Nanjing University of Industry Technology and the Natural Science Foundation of Jiangsu Province, China under Grant BK20230309.

Conflicts of Interest

The authors declare no conflicts of interest.

AI Use Statement

The authors declare that no generative AI was used in the preparation of this manuscript.

Ethical Approval and Consent to Participate

Not applicable.

References

[1] Rani, P., & Nagaraja, C. M. (2026). A comprehensive review on development of framework-(MOF/COF/POP) based materials for catalytic conversion of carbon dioxide from dilute/flue gas sources to high-value chemicals. *Coordination Chemistry Reviews, 561*, 217896. [CrossRef]

[2] Zhou, J., Li, J., Kan, L., Zhang, L., Huang, Q., Yan, Y., ... & Lan, Y. Q. (2022). Linking oxidative and reductive clusters to prepare crystalline porous catalysts for photocatalytic CO2 reduction with H2O. *Nature Communications, 13*(1), 4681. [CrossRef]

[3] Yan, S., Wan, L., Li, Z., & Zou, Z. (2011). Facile temperature-controlled synthesis of hexagonal Zn2GeO4nanorods with different aspect ratios toward improved photocatalytic activity for overall water splitting and photoreduction of CO2. *Chemical communications, 47*(19), 5632-5634. [CrossRef]

[4] He, Y., Chen, C., Liu, Y., Yang, Y., Li, C., Shi, Z., ... & Feng, S. (2022). Quantitative evaluation of carrier dynamics in full-spectrum responsive metallic ZnIn2S4 with indium vacancies for boosting photocatalytic CO2 reduction. *Nano letters, 22*(12), 4970-4978. [CrossRef]

[5] Gao, W., Li, S., He, H., Li, X., Cheng, Z., Yang, Y., Shen, Q., Wang, X., Xiong, Y., Zhou, Y., & Zou, Z. (2021). Vacancy-defect modulated pathway of photoreduction of CO_2 on single atomically thin $AgInP_2S_6$ sheets into olefin gas. *Nature Communications, 12*, 4747. [CrossRef]

[6] Sun, J., Bai, Y., Feng, X., Liu, D., & Zhang, Y. (2025). Zn2GeO4@ CeO2 core@ shell nanorods for efficient photocatalytic CO2 reduction. *Molecules, 30*(10), 2205. [CrossRef]

[7] Zhang, N., Ouyang, S., Li, P., Zhang, Y., Xi, G., Kako, T., & Ye, J. (2011). Ion-exchange synthesis of a micro/mesoporous Zn2GeO4 photocatalyst at room temperature for photoreduction of CO2. *Chemical Communications, 47*(7), 2041-2043. [CrossRef]

[8] de Conti, M. C. M. D., Camargo, L. P., da Silva Fabris, G., da Silva, P. R. C., de Santana, H., Fernandes, R. V., ... & La Porta, F. D. A. (2024). Hydrothermal growth of Zn2GeO4 nanorods for optical and (Photo) Catalytic applications: An experimental and theoretical study. *Materials Today Chemistry, 41*, 102313. [CrossRef]

[9] Liu, L., Fan, W., Zhao, X., Sun, H., Li, P., & Sun, L. (2012). Surface dependence of CO_2 adsorption on Zn_2GeO_4. *Langmuir, 28*(28), 10415-10424. [CrossRef]

[10] Wang, G., Lv, S., Shen, Y., Li, W., Lin, L., & Li, Z. (2024). Advancements in heterojunction, cocatalyst, defect and morphology engineering of semiconductor oxide photocatalysts. *Journal of Materiomics, 10*(2), 315-338. [CrossRef]

[11] Wang, J., Asakura, Y., & Yin, S. (2020). Synthesis of zinc germanium oxynitride nanotube as a visible-light driven photocatalyst for NO_x decomposition through ordered morphological transformation from Zn_2GeO_4 nanorod obtained by hydrothermal reaction. *Journal of Hazardous Materials, 396*, 122709. [CrossRef]

[12] Gao, W., Chi, H., Xiong, Y., Ye, J., Zou, Z., & Zhou, Y. (2024). Comprehensive insight into construction of active sites toward steering photocatalytic CO2 conversion. *Advanced Functional Materials, 34*(13), 2312056. [CrossRef]

[13] Liang, J., Chai, Y., Li, L., Li, D., Shen, J., Zhang, Y., & Wang, X. (2020). Germanium and iron double-substituted ZnGa2O4 solid-solution photocatalysts with modulated band structure for boosting photocatalytic CO2 reduction with H2O. *Applied Catalysis B: Environmental, 265*, 118551. [CrossRef]

[14] Liu, Q., Zhou, Y., Tian, Z., Chen, X., Gao, J., & Zou, Z. (2012). Zn_2GeO_4 crystal splitting toward sheaf-like, hyperbranched nanostructures and photocatalytic reduction of CO_2 into CH_4 under visible light after nitridation. *Journal of Materials Chemistry, 22*(5), 2033–2038. [CrossRef]

[15] Zhao, W., Zhang, C., Shi, Y., Wu, R., & Zhang, B. (2015). Self-assembled synthesis of hierarchical Zn_2GeO_4 core–shell microspheres with enhanced photocatalytic activity. *Dalton Transactions, 44*(1), 75–82. [CrossRef]

[16] Liang, J., Xu, J., Long, J., Zhang, Z., & Wang, X. (2013). Self-assembled micro/nano-structured Zn_2GeO_4 hollow spheres: direct synthesis and enhanced photocatalytic activity. *Journal of Materials Chemistry A, 1*(36), 10622–10625. [CrossRef]

[17] Liu, J., & Zhang, G. (2013). Template-free synthesis and high photocatalytic activity of hierarchical Zn_2GeO_4 microspheres. *CrystEngComm, 15*(2), 382–389. [CrossRef]

[18] Zhang, Q., Pang, K., & Xu, Y. (2018). Controlled synthesis of Bi_2O_3/BiOBr/Zn_2GeO_4 heterojunction photocatalysts with enhanced photocatalytic activity. *Journal of the American Ceramic Society, 101*(12), 5858. [CrossRef]

[19] Yuan, Y., Zhou, B., Ding, C., Chi, H., Gao, W., Zhou, Y., & Zou, Z. (2025). Nano forests for artificial photosynthesis: growth of high-density vertically aligned zinc germanate nanoribbons promoting CO2 photoconversion into solar fuels. *Materials Letters*, 139294. [CrossRef]

[20] Xu, X., Zou, J., Xiao, Z., Wang, B., Jiang, J., Shen, J., ... & Zhang, Z. (2025). Crystalline ZnO aerogel microspheres for boosting photocatalytic CO2 reduction. *Fuel, 398*, 135519. [CrossRef]

[21] Zhao, W., Ren, S., Zheng, Y., Sun, Y., Wu, X., Liu, C., ... & Shen, X. (2025). Regulating a Co3O4/ZnO heterojunction aerogel with a built-in electric field for enhanced CO2 photoreduction to solar fuels from DFT insights. *Nanoscale, 17*(28), 16725-16736. [CrossRef]

[22] Liu, W., Zhou, T., Zheng, Y., Liu, J., Feng, C., Shen, Y., Huang, Y., & Guo, Z. (2017). Hierarchical structural evolution of Zn_2GeO_4 in binary solvent and its effect on Li-ion storage performance. *ACS Applied Materials & Interfaces, 9*(11), 9778. [CrossRef]

[23] Yan, S., Wang, J., & Zou, Z. (2013). An anion-controlled crystal growth route to Zn2GeO4 nanorods for efficient photocatalytic conversion of CO2 into CH4. *Dalton Transactions, 42*(36), 12975-12979. [CrossRef]

[24] Liu, Q., Zhou, Y., Kou, J., Chen, X., Tian, Z., Gao, J., Yan, S., & Zou, Z. (2010). High-yield synthesis of ultralong and ultrathin Zn_2GeO_4 nanoribbons toward improved photocatalytic reduction of CO_2 into renewable hydrocarbon fuel. *Journal of the American Chemical Society, 132*(41), 14385-14387. [CrossRef]

[25] Fu, Z., Zhao, X., Zhang, S., & Fu, Z. (2021). Preparation of nano-Zn2GeO4/rGO composite photocatalyst and its treatment of synthetic dye wastewater. *Materials Chemistry and Physics, 259*, 124004. [CrossRef]

[26] Deng, Z. X., Wang, C., Sun, X. M., & Li, Y. D. (2002). Structure-directing coordination template effect of ethylenediamine in formations of ZnS and ZnSe nanocrystallites via solvothermal route. *Inorganic Chemistry, 41*(4), 869-873. [CrossRef]

[27] Ma, Z., Liu, X., Wang, X., Luo, Z., Li, W., Nie, Y., Pei, L., Mao, Q., Wen, X., & Zhong, J. (2023). Manipulating the d-band center enhances photoreduction of CO_2 to CO in Zn_2GeO_4 nanorods. *Chemical Engineering Journal, 468*, 143569. [CrossRef]

[28] Manna, R., Rahut, S., & Samanta, A. N. (2023). Synergistic effect of Zn_2GeO_4 nanorod decorated metal organic framework ZIF-67 and its metal ligand charge transfer effect towards the photocatalytic CO_2 reduction and C–C coupling. *Materials Today Energy, 35*, 101326. [CrossRef]

[29] Zhao, H., Wang, X., Feng, J., Chen, Y., Yang, X., Gao, S., & Cao, R. (2018). Synthesis and characterization of Zn_2GeO_4/Mg-MOF-74 composites with enhanced photocatalytic activity for CO_2 reduction. *Catalysis Science & Technology, 8*(5), 1288–1295. [CrossRef]

[30] Han, Z., Zhao, Y., Gao, G., Zhang, W., Qu, Y., Zhu, H., Zhu, P., & Wang, G. (2021). Erbium single atom composite photocatalysts for reduction of CO_2 under visible light: CO_2 molecular activation and 4f levels as an electron transport bridge. *Small, 17*(26), 2102089. [CrossRef]

[31] Liu, Q., Low, Z.-X., Li, L., Razmjou, A., Wang, K., Yao, J., & Wang, H. (2013). ZIF-8/Zn_2GeO_4 nanorods with an enhanced CO_2 adsorption property in an aqueous medium for photocatalytic synthesis of liquid fuel. *Journal of Materials Chemistry A, 1*(38), 11563–11569. [CrossRef]

Yiqing Wei Ph.D., is a lecturer at Nanjing University of Industry Technology. Her research direction is the design of photocatalytic material systems and the regulation of their performance. (Email: wyq@niit.edu.cn)

Chen Zhuang is a doctoral candidate at Nanjing University, with his main research focus placed on the applied research of photocatalytic systems targeted at carbon cycling conversion and renewable energy utilization. (Email: zhch2020@smail.nju.edu.cn)

Wei Zhao received the B.S. degree from Nanjing University, specializing in the research field of photocatalytic materials. (Email: 221840261@smail.nju.edu.cn)

Yong Zhou is a professor at the Environmental Ecomaterials and Renewable Energy Research Center of Nanjing University. His primary research interests lie in artificial photosynthesis, which targets the highly efficient conversion of CO_2 into renewable hydrocarbon fuels via well-engineered photocatalytic systems. (Email: zhouyong1999@nju.edu.cn)